# Validity of the Keller-Miksis equation for ”non-stable” cavitation and the acoustic emissions generated

Kristoffer Johansen, Jae Hee Song, and Paul Prentice
CavLab, Medical and Industrial Ultrasonics, School of Engineering
University of Glasgow, Glasgow, G12 8QQ, United Kingdom
Email: Paul.Prentice@glasgow.ac.uk

***Abstract*—The Keller-Miksis equation (KME) is commonly used for numerical studies of inertial and stable-inertial cavitation. However, experimental validation of KME under clinically relevant exposure settings is scarce, particularly in terms of the acoustic emission signal generated by the cavitation. In this paper, the KME is validated against a cavitation cloud collapsing $f_0/2$ and $f_0/3$ sub-harmonically with some success. This could significantly aid the design of arrays for passive acoustic mapping (PAM), quantification of cavitation dose, and tuning controllers for feed-back-loops.**

## I. Introduction

Cavitation is being applied in both medicine and industry, for which the acoustic emissions, and the spectrum associated with them, are used as a concise summary, both for classification of cavitation regime and quantification [1]–[3].

We have recently published an analysis of the acoustic cavitation noise spectrum, where we identify the role of periodic shock waves (PSWs), that are emitted from a stable–inertially collapsing cavitation cloud [4]. It shows that all spectral features, expect parts of the fundamental frequency, are mediated by PSWs. The physical interpretation of the collected emissions was only made possible after the complex impulse response to the needle hydrophone (NH) was removed from the collected emissions [5]. Furthermore, we have shown that spatially configured cavitation clouds can be positioned such that sub-harmonic ($f_0/n$ and $n \in \mathbb{N}$ and $f_0$ is the fundamental driving frequency), and ultra-harmonic spectral features ($m\, f_0/n$ for $n \neq m$ and $m \in \mathbb{N}$), are suppressed below the detection threshold.

Cavitation clouds are commonly described through rather complex theoretical considerations [6], however, for certain cavitation activity in high-intensity focused ultrasound (HIFU) fields, where the cavitation clouds are closely packed, the overall complexity of the system might be reduced. Therefore, to expedite the route from the laboratory to applications, we are suggesting that applying Rayleigh–Plesset-like equations and computing the acoustic emissions generated, could assist in design of control systems used to monitor cavitation mediated effects.

In [4] the individual PSWs are fitted manually, achieving a high similarity between the synthetic signal and its spectrum when compared to the experimental measurement. In this paper we investigate the validity of the Keller-Miksis equation, and computed acoustic emissions, high-speed imaging data and acoustic data from a calibrated NH are used for respective validation. Two sub-harmonic regimes are represented, $f_0/2$ and $f_0/3$, to evaluate the power of the simplifying assumption; a cavitation cloud can be approximated as a single-bubble for several cycles of stable–inertial cavitation.

## II. Methods

The experimental arrangement used in this paper is fully described in [4], Fig. 1 (a). We employ the laser-nucleation technique [7], to precisely initiate cavitation activity relative to the NH tip, and in the HIFU focus. HIFU is generated via a single element piezoceramic transducer (H-149, Sonic Concepts, USA), connected to a power amplifier (2100L, Electronic and Innovation, USA) and a waveform generator (DG4102, Rigol Technologies, China). The transducer is geometrically focused to 68 mm from the front face, and it is driven at the 3rd harmonic through an impedance matching network, such that $f_0 = 698$ kHz for all results presented. This driving frequency is well within the calibration bandwidth of the NH (1.0 mm diameter, PVdF, Precision Acoustics, UK) ensuring that acoustic cavitation emissions are adequately detected, processed and interpreted [5]. A 20 mm central hole, through the body of the transducer, serves to mount the NH in emission collection postion, Fig 1 (b), aligned vertically along the HIFU axis, Fig. 1 (a), with the tip located around the pre-focus $-6$ dB contour, $\sim 3$ mm from the focal point. The NH is connected to an oscilloscope (MS07104A, Agilent Technologies, USA), and data collected at 4 GSs$^{-1}$. The HIFU field is somewhat perturbed by the presence of a NH, decreasing the pressure by $\sim 15\%$, compared to no NH in the emission collection position. This is assessed in detail with a fiber-optic hydrophone in [4].

The nucleation laser emits a single $1.2 \pm 0.1$ mJ (instrument error according to manufacturer), $6 - 8$ ns laser pulse (Nano S 130-10 frequency doubled Q-switched Nd:YAG, Litron Lasers, UK), that is passed through a long working distance microscope objective lens (50x 0.42 NA Mitutoyo, Japan), submerged in a sealed unit, mounted on an xyz-manipulator (Velmex Motor, Bloomfield, NY, USA), and pre-aligned to the HIFU focus, $\sim 3$ mm above the NH tip in-situ. The laser

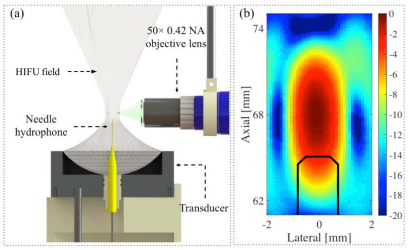


Fig. 1. Illustration of experimental setup: (a) cross-sectional side view, and (b) an axial scan of the HIFU focal region, with representations of the NH outlined for 'emission collection' position (solid black).

pulse, triggered to be incident $\sim 5$ cycles into a 65-cycle burst of HIFU, generated the cavitation activity reported below in free-field driving conditions [7].

The transducer-NH configuration is housed within a custom-built chamber, measuring $420 \times 438 \times 220\,\mathrm{mm}^3$ and filled with degassed, deionized water. Imaging optics are placed within the two recessed walls, in close proximity to the intended location of the cavitation cloud, facilitating reasonably high spatial resolution imaging.

High-speed shadowgraphic imaging of the resulting cavitation activity is undertaken orthogonally to the nucleating laser axis, through a Monozoom 7 lens system (Bausch & Lomb, USA), at $5 \times 10^6$ frames per-second (HPV-X2, Shimadzu, Japan), with synchronous 10 ns laser pulses (CAVILUX Smart, Cavitar, Finland) providing the illumination and effective temporal resolution, per frame. A delay generator (DG535, Stanford Research Systems, USA) provides electronic triggering to synchronize each of the instruments. The Q-switch from the nucleation laser, which is detected by the NH, signifies laser pulse emission, and is taken as $t = 0\,\mu$s.

Assuming that the cavitation clouds generated are closely packed, and component bubbles are in phase with each other, a single-bubble model is used to describe the phenomenon, to first order. For this work, the Keller–Miksis equation (KME) was applied, as it is specifically derived for inertial bubble dynamics, in which the compressibility of the host medium influences the temporal evolution of the bubble. The KME can be expressed the following way:

$$\left(1-\frac{\dot{R}}{c}\right)R\ddot{R}+\left(\frac{3}{2}-\frac{\dot{R}}{2c}\right)\dot{R}^2=\frac{1}{\rho}\left(1+\frac{\dot{R}}{c}\right)p_\mathrm{w}+\frac{R}{\rho c}\frac{dp_\mathrm{w}}{dt}\ , \quad (1)$$

where $R$ is the instantaneous radius, and the dots indicate time derivatives, $c$ is the speed of sound, and $p_\mathrm{w}$ is the pressure at the bubble wall, which can be expressed as [8]:

$$p_\mathrm{w}=\left(P_0+\frac{2\sigma}{R_0}\right)\left(\frac{R_0}{R}\right)^{3\kappa}-\frac{2\sigma}{R}-\frac{4\eta\dot{R}}{R}-P_0-P_\mathrm{a}\sin(\omega t)\ , \quad (2)$$

where $\sigma$ is the surface tension between the gas–water interface, $R_0$ is the equilibrium radius, $\kappa$ is the polytropic exponent, and $P_\mathrm{a}$ is the pressure amplitude of the driving HIFU. From the solution of Eq. (1), the acoustic emission $P_\mathrm{rad}$ are computed. This can be expressed the following way [9]:

$$P_\mathrm{rad}=\rho\frac{R^2\ddot{R}+2R\dot{R}^2}{r}\ , \quad (3)$$

where $r$ is the distance from the bubble centre to the NH. The computed acoustic emissions are compared to the physically detected acoustic emissions, with the NH. The acoustic emissions collected by the NH are deconvolved with the complex frequency response to the NH, to correct for any distortions coming from the NH [5]. In the frequency-domain, the magnitude of the acoustic emissions $|P_\mathrm{rad}|$, are expressed as [10]:

$$|P_\mathrm{rad}|=\frac{|U_\mathrm{NH}|}{|H_\mathrm{NH}||H_\mathrm{bpf}|}\ , \quad (4)$$

where $|H_\mathrm{NH}|$ is the magnitude of the frequency response to the NH, $|U_\mathrm{NH}|$ is the magnitude of the voltage–trace, and $|H_\mathrm{bpf}|$ is the magnitude of the brick wall bandpass filter used, equal to that seen in [5], Fig. 4. The limits of the bandpass filter are equal to the calibration bandwidth ($125\,\mathrm{kHz} - 20\,\mathrm{MHz}$) to the NH.

## III. Results and Discussion

### A. $f_0/2$ *regime*

Figures 2(a) show high-speed imaging data captured of a cavitation cloud oscillating in a HIFU field of free-fild driving amplitude $P_\mathrm{a} = 1.63 \pm 0.12\,\mathrm{MPa}$. The images confirms, that to first approximation, a cavitation cloud can be described as a single-bubble, for the initial cycles of inertial deflation and compression. Figure 3(a) represents the normalised dark-pixel count from the high-speed images, where the dark-pixel count represent how the cavitation cloud is collapsing sub-harmonically at $f_0/2$, with the emission of PSWs, which are also depicted in the imaging data as a result of the shadowgraphic capabilities. To enhance the shadowgraphic performance of the set-up, the optical focus is placed slightly off from the plane of the bubble, causing the bubble to be sub-optimally resolved [11]. In part for this reason, the dark-pixel data is presented in normalised form, implying that it can only be used to compare relative temporal evolution between experiment and simulation. The simulated radius-time curve in Fig. 3(a), shows that the solution of Eq. (1) is to a large extent, in agreement with the temporal profile of the dark-pixel count, both with regards to collapse times and the oscillations between collapses, however, it is solved with a driving pressure which is 0.19 MPa lower than what is suggested by that measured with the fibre-optic hydrophone. This difference could potentially be explained by the fibre-optic hydrophone being placed slightly off from the plane where the bubble was oscillating. An alternative explanation would be that the pressure was in fact higher, and the KME is not sufficiently describing the radial dynamics of the cavitation cloud.

Figure 3(b) is the deconvolved acoustic emissions collected by the NH. For the emissions presented, a control experiment has been subtracted, where the nucleation laser was not fired,

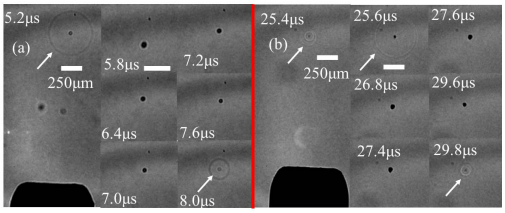


Fig. 2. (a) High-speed images of a single $f_0/2$ cavitation event, 2.7 mm from NH tip. (b) High-speed images of a single $f_0/3$ cavitation event, 2.5mm from NH tip.

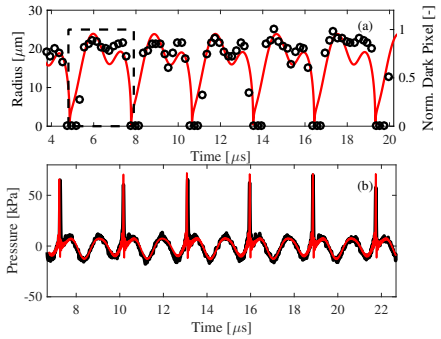


Fig. 3. (a) (left) Simulated radius-time curve from KME (red), with dashed rectangle representing the sub-harmonic oscillation imaged, and (right) normalised dark-pixel count (black scatter) from images in Fig. 2(a). (b) Acoustic emissions from the driven bubble, measured by the NH (black) and simulated (red), with periodic shock wave features arrowed from collapses in (b).The KME is solved with the following parameters: $R_0 = 3\,\mu$m, $\rho = 998\,\mathrm{kgm}^{-3}$, $\mu = 0.001\,Pa\,s$, $\sigma = 0.072\mathrm{N\,m}^{-1}$ $c = 1484\,\mathrm{ms}^{-1}$, $P_0 = 101\,$kPa, $P_\mathrm{a} = 1.31\,$MPa, $R(0) = 3\,\mu$m, and $\dot{R}(0) = 0\,\mathrm{ms}^{-1}$

to remove the primary HIFU field. The acoustic emissions consists of 6 PSW of average peak positive pressure amplitude $\mathrm{PPPA_{PSW}} = 63.5 \pm 4.3\,$kPa, originating from the respective collapses of the cavitation cloud, 2.7 mm away from the NH. The oscillation between collapses in Fig. 3(a) is acoustically manifested by emissions, primarily consisting of the fundamental frequency. This is to be expected as the oscillation between collapses is of small amplitude, and to first approximation it is linear. The acoustic emissions computed from Eq. (3) are also shown in Fig. 3(b), in which the temporal evolution is to first order in agreement with the experimental data. However, the $\mathrm{PPPA_{PSW}}$ is somewhat higher, $\mathrm{PPPA_{PSW}} = 70.1 \pm 2.5\,$kPa, and fundamental emission from between collapses is slightly lower.

Figure 4 shows the spectra of the experimentally measured acoustic emissions and the simulated emission from Fig. 3(c). As discussed in [4], all spectral features except parts of the fundamental come from PSWs. Attempting to simulate a series of shock waves, and replicating the spectral features, is to a lesser extent achieved with the presented approach, compared to fitting individual bubble-collapse shock waves manually [4]. Nevertheless, it is appreciated that the crude simulation of the stable–inertially collapsing cavitation cloud is reproducing all spectral features within 3 dB, up to the 11 $f_0/2$ harmonic of the sub-harmonic. From which it is reasonable to suggest that

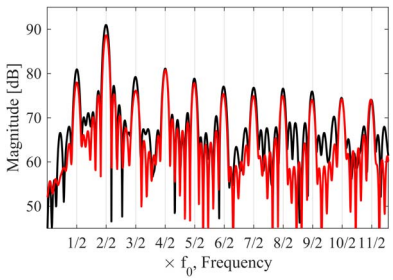


Fig. 4. Spectra of acoustic emissions in Fig 3 (b), where measured by NH (black) and simulated (red).

KME is to first order approximating the radial dynamics of the cavitation cloud.

### *B. $f_0/3$ regime*

When the pressure amplitude of the HIFU field is increased to $P_\mathrm{a} = 2.40 \pm 0.09\,$MPa, the cavitation cloud starts to collapse every third cycle. This is consistent with previous reports, where increasing the pressure amplitude of the driving field excites higher sub-harmonics [12]. The cavitation cloud seen in Fig 2(b) is now larger, compared to Fig. 2(a), and the images are also suggesting that the cloud is now consisting of a set of component bubbles, as it is more non-spherical. This is of course alluding to, that the assumption of the cavitation cloud, more than less is behaving as a single-bubble, could be of diminishing validity. This concern is further supported by the double-fronted shock waves, at 25.4 $\mu$s and 25.6 $\mu$s, which is indicating that the component bubbles are not collapsing in-phase. This is a feature that a single-bubble model does not support.

Figure 5(a) represents the normalised dark-pixel count and the KME simulation, in which it is reasonable to state that the simulation and the experimental data mimics the same trends, and collapse times are to first order in agreement. However, it is also worth noting that, compared to the $f_0/2$ results in Fig. 3(a), the agreement is less satisfying. The dark-pixel data indicates that the cavitation cloud is slightly growing, just over this small time period. An alternative explanation would be that the component bubbles are less closely packed after a certain number inertial collapses, making the cavitation cloud more non-spherical and appear larger. In any case, this is not something the current KME model adopted can replicate.

Similarly, for the acoustic emissions detected by the NH, and the computed acoustic emissions from Eq. (3), there is a much larger discrepancy between the two, compared to the results presented in Fig. 3(b). The experimental data has PSWs with average amplitude $\mathrm{PPPA_{PSW}} = 108.1 \pm 11.9\,$kPa, and the simulation has $\mathrm{PPPA_{PSW}} = 172.5 \pm 20.5\,$kPa, showing that the simulation is again consistently overestimating the PSW pressure amplitude. This is ultimately indicating that the KME is less satisfactorily describing the temporal evolution of this cavitation cloud. Potentially, this could be related to that the cavitation cloud is collapsing harder, and more non-linearly, seen from the stronger acoustic emissions, where

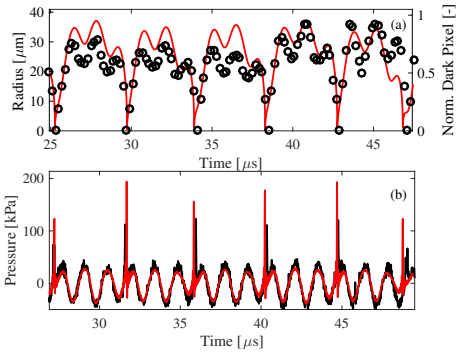


Fig. 5. (a) (left)Simulated radius-time curve from KME, with dashed rectangle representing the sub-harmonic oscillation imaged, and (right) normalised dark-pixel count (black scatter) from images in Fig. 2 (b). (b) Acoustic emissions from the driven bubble, measured by the NH (grey) and simulated (red), with periodic shock wave features arrowed from collapses in (b). The KME is solved with the following parameters: $R_0 = 6\,\mu$m, $\rho = 998\,\mathrm{kgm}^{-3}$, $\mu = 0.001\,Pa\,s$, $\sigma = 0.072\mathrm{N\,m}^{-1}$ $c = 1484\,\mathrm{ms}^{-1}$, $P_0 = 101\,$kPa, $P_\mathrm{a} = 2.40\,$MPa, $R(0) = 6\,\mu$m, and $\dot{R}(0) = 0\,\mathrm{ms}^{-1}$

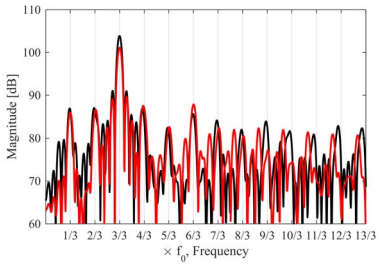


Fig. 6. Spectra of acoustic emissions in Fig 5 (b), where measured by NH (black) and simulated (red).

the KME is not able to capture the totality of the dynamics adequately.

Figure 6 contains the spectra of the emissions in Fig. 5(b), and up to the second harmonic of the fundamental the agreement is reasonable. For higher frequency content, as should be expected, the agreement between the two spectra is significantly worse, compared to Fig. 4. This is due to the fact that the timings between respective shocks are not well replicated between the two representations, and therefore high frequency content is not adding at the correct phases in the simulated acoustic emissions [4, 13]. From the results presented in Fig. 6 it is reasonable to state that the KME and Eq. (3) are convincingly describing the acoustic emissions up to the second harmonic of the fundamental.

With regards to using the KME, and Eq. (3) to investigate control feed-back-loops, it seems to be reasonable to suggest that it would be an excellent pursuit, if the control protocol chosen is focused on spectral features close to the fundamental. This could indeed also be used for the design, and full-system descriptions of PAM systems that are attempting to control some cavitation activity. Use of Rayleigh–Plesset-like equations can also be used to aide work related to quantifying cavitation doses, both for treatment planning and evaluating the treatment given.

## IV. Conclusion

For $f_0/2$ sub-harmonic cavitation cloud behaviour, the KME and Eq. (3) are performing reasonably over a wide bandwidth, however, there are discrepancies. For higher HIFU driving pressures, where the cavitation cloud is collapsing at $f_0/3$, the behaviour is less satisfactorily described, as the cavitation cloud is failing to satisfy the single-bubble assumption. However, even at $f_0/3$ oscillations, acoustic emissions up to the second harmonic of the fundamental are well replicated with the suggested theory. This is indicating that the KME can be used in the design and tuning of controllers for feed-back-loops.

## Acknowledgement

The research leading to these results has received funding from the European Research Council under the European Unions Seventh Framework Programme (FP/2007 2013)/ERC Grant Agreement no. 336189 (TheraCav). The authors acknowledge Graeme Casey and Miriam Jiménez García for technical assistance.

## References

[1] C. M. Schoellhammer, A. Schroeder, R. Maa, G. Y. Lauwers, A. Swiston, M. Zervas, R. Barman, A. M. DiCiccio, W. R. Brugge, D. G. Anderson, D. Blankschtein, R. Langer, and G. Traverso, "Ultrasound-mediated gastrointestinal drug delivery." *Science translational medicine*, vol. 7, no. 310, p. 310ra168, 2015.

[2] M. A. O'Reilly and K. Hynynen, "Blood-Brain Barrier: Real-time Feedback-controlled Focused Ultrasound Disruption by Using an Acoustic Emissions-based Controller," *Radiology*, vol. 263, no. 1, pp. 96–106, 2012.

[3] L. K. Tompson, L. H., Doraiswamy, "Sonochemistry: Science and Engineering," *Ind. Eng. Chem. Res.*, vol. 38, pp. 1215 – 1249, 1999.

[4] J. H. Song, K. Johansen, and P. Prentice, "An analysis of the acoustic cavitation noise spectrum : The role of periodic shock waves," *Journal of Acoustical Soceity of America*, vol. 140, pp. 2494 – 2505, 2016.

[5] K. Johansen, J. H. Song, K. Johnston, and P. Prentice, "Deconvolution of acoustically detected bubble-collapse shock waves," *Ultrasonics*, vol. 73, pp. 144–153, 2017.

[6] Y.-C. Wang and C. E. Brennen, "Numerical Computation of Shock Waves in a Spherical Cloud of Cavitation Bubbles," *Journal of Fluids Engineering*, vol. 121, no. 4, p. 872, 1999.

[7] B. Gerold, S. Kotopoulis, C. McDougall, D. McGloin, M. Postema, and P. Prentice, "Laser-nucleated acoustic cavitation in focused ultrasound," *Review of Scientific Instruments*, vol. 82, no. 4, 2011.

[8] K. Ando, T. Colonius, and C. E. Brennen, *Bubble Dynamics and Shock Waves*, 2013. [Online]. Available: http://link.springer.com/10.1007/978-3-642-34297-4

[9] C. E. Brennen, "Cavitation in medicine," *Interface Focus*, vol. 5, no. 5, p. 20150022, 2015.

[10] A. Hurrell and S. Rajagopal, "The practicalities of obtaining and using hydrophone calibration data to derive pressure waveforms," *IEEE Transactions on Ultrasonics, Ferroelectrics, and Frequency Control*, 2016. [Online]. Available: http://ieeexplore.ieee.org/lpdocs/epic03/wrapper.htm?arnumber=7523441

[11] N. Kudo, "A Simple Technique for Visualizing Ultrasound Fields Without Schlieren Optics," *Ultrasound in Medicine & Biology*, vol. 41, no. 7, pp. 2071–2081, 2015.

[12] W. Lauterborn and E. Cramer, "Subharmonic route to chaos observed in acoustics," *Physical Review Letters*, vol. 47, no. 20, pp. 1445–1448, 1981.

[13] J. H. Song, K. Johansen, and P. Prentice, "Covert cavitation : Spectral peak suppression in the acoustic emissions from spatially configured nucleations," *Journal of Acoustical Soceity of America*, vol. 141, no. 3, pp. EL216–EL221, 2017.